Imaging Features in the Liver after Stereotactic Body Radiation Therapy

Patrick J. Navin, MB, BCh, BAO
Michael C. Olson, MD
Mishal Mendiratta-Lala, MD
Christopher L. Hallemeier, MD
Michael S. Torbenson, MD
Sudhakar K. Venkatesh, MD

Abbreviations: ADC = apparent diffusion coefficient, APHE = arterial phase hyperenhancement, EBRT = external-beam radiation therapy, FLR = focal liver reaction, HCC = hepatocellular carcinoma, LI-RADS = Liver Imaging Reporting and Data System, RILD = radiation-induced liver disease, SBRT = stereotactic body radiation therapy

RadioGraphics 2022; 42:0000–0000

https://doi.org/10.1148/rg.220084

Content Codes: GI OI RO

From the Departments of Radiology (P.J.N., M.C.O., S.K.V.), Radiation Oncology (C.L.H.), and Pathology (M.S.T.), Mayo Clinic, 200 First St SW, Rochester, MN 55905; and Department of Radiology, University of Michigan, Ann Arbor, Mich (M.M.L.). Recipient of a Certificate of Merit award for an education exhibit at the 2021 RSNA Annual Meeting. Received April 11, 2022; revision requested May 12 and received May 25; accepted June 3. For this journal-based SA-CME activity, the author S.K.V. has provided disclosures (see end of article); all other authors, the editor, and the reviewers have disclosed no relevant relationships. **Address correspondence to** P.J.N. (email: *navin.patrick@mayo.edu*).

SA-CME LEARNING OBJECTIVES

After completing this journal-based SA-CME activity, participants will be able to:

- Explain the general principles of SBRT.
- Describe the indications for SBRT in the liver and its associated efficacy.
- Identify the imaging features in a liver tumor and surrounding parenchyma after SBRT with emphasis on potential pitfalls and complications.

See rsna.org/learning-center-rg.

Historically, radiation therapy was not considered in treatment of liver tumors owing to the risk of radiation-induced liver disease. However, development of highly conformed radiation treatments such as stereotactic body radiation therapy (SBRT) has increased use of radiation therapy in the liver. SBRT is indicated in treatment of primary and metastatic liver tumors with outcomes comparable to those of other local therapies, especially in treatment of hepatocellular carcinoma. After SBRT, imaging features of the tumor and surrounding background hepatic parenchyma demonstrate a predictable pattern immediately after treatment and during follow-up. The goals of SBRT are to deliver a lethal radiation dose to the targeted liver tumor and to minimize radiation dose to normal liver parenchyma and other adjacent organs. Evaluation of tumor response after SBRT centers on changes in size and enhancement; however, these changes are often delayed secondary to the underlying physiologic effects of radiation. Knowledge of the underlying pathophysiologic mechanisms of SBRT should allow better understanding of the typical imaging features in detection of tumor response and avoid misinterpretation from common pitfalls and atypical imaging findings. Imaging features of radiation-induced change in the surrounding liver parenchyma are characterized by a focal liver reaction that can potentially be mistaken for no response or recurrence of tumor. Knowledge of the pattern and chronology of this phenomenon may allay any uncertainty in assessment of tumor response. Other pitfalls related to fiducial marker placement or combination therapies are important to recognize. The authors review the basic principles of SBRT and illustrate post-SBRT imaging features of treated liver tumors and adjacent liver parenchyma with a focus on avoiding pitfalls in imaging evaluation of response.

Online supplemental material is available for this article.

Introduction

Primary liver cancer accounted for 2.2% of all new cancer cases in the United States in 2021 and for 5% of cancer deaths (1). Liver metastases were present in 5.1% of all cancer patients in the United States on the basis of figures from the Surveillance, Epidemiology, and End Results (SEER) program of the National Cancer Institute (2). Surgery is considered the optimal treatment for management of primary or metastatic liver tumors. However, surgery is often not an option owing to patient conditions, tumor multifocality, tumor location, or liver functional reserve.

For this reason, less invasive options have emerged for local treatment of hepatic tumors. These are generally divided into three main categories: percutaneous ablation (radiofrequency ablation, microwave ablation, cryoablation, ethanol ablation, irreversible electroporation), arterial-based embolic therapies (bland embolization, chemoembolization, radioembolization with yttrium 90), and radiation therapy.

TEACHING POINTS

- The aim of SBRT is to deliver highly conformed radiation to the target tumor while achieving rapid dose falloff to minimize damage to surrounding normal or nontumor tissue.
- The direct mechanism of cell death occurs secondary to double-stranded breaks in DNA and results in cell death. Indirect mechanisms are believed to arise from vascular damage and antitumor immune response, in which the tumor cells remain metabolically active after treatment until eventual cell death.
- Therefore, assessment of tumor size in grading response in the first 6–12 months demonstrates poor accuracy, often related to persistent viable tumor and necrosis, given the pathophysiology of radiation-induced cell death.
- Although reduced enhancement is historically a biomarker of response in hepatic tumors, SBRT-treated liver malignancies often show persistent enhancement in the early posttreatment phase, which can last up to and beyond 1 year and should not be mistaken for viable tumor that needs treatment.
- Close review of the radiation planning images and pretreatment images is useful to understand the radiation field, which should correlate with the imaging appearance of FLR.

Use of external-beam radiation therapy (EBRT) in treatment of liver tumors has had a limited role until recent years because of radiation-induced liver disease (RILD) at even minimal doses (3). However, recent advances in diagnostic imaging, EBRT targeting, and EBRT delivery have allowed EBRT to reemerge as a potential treatment method for primary or metastatic liver cancer. Stereotactic body radiation therapy (SBRT) is one such EBRT method that has demonstrated efficacy in recent years.

In this review, we examine the basic principles of SBRT and identify imaging features that help in assessment of treatment response, with a focus on potential pitfalls and complications.

Stereotactic Body Radiation Therapy

SBRT is defined as the EBRT method used to very precisely deliver a high dose of radiation, either as a single dose or divided into three to five fractions (hypofractionated dose) (4). This method was first developed for intracranial indications, with its first use for intracranial metastases described in 1975 at the Karolinska Institute in Sweden (5). Owing to issues with patient motion and tumor localization, technical advances were required to allow extracranial stereotactic radiation therapy to commence. Abdominal tumors can move up to 25 mm with regular breathing and 55 mm with deep breathing; thus, new methods were developed to minimize motion and allow safe administration of radiation (6).

Basic Principles

The aim of SBRT is to deliver highly conformed radiation to the target tumor while achieving rapid dose falloff to minimize damage to surrounding normal or nontumor tissue (7). This rapid falloff is achieved by using multiple beams targeted to the tumor over a large circumferential angular range. Treatments are given over a single fraction or multiple fractions. SBRT employs higher doses per fraction (typically >6 Gy per fraction) than were historically used with conventional fractionation (1.8–2 Gy per fraction). In the United States, commercial and government payers define SBRT as involving up to five fractions in a treatment course; however, in other countries, treatment courses of greater than five fractions may be used.

SBRT may use high-dose x-ray photons or accelerated protons to deliver its treatment dose (Fig 1). Photon delivery is a commonly used tool for multiple malignancies, cost-effective and supported by high-level evidence (8,9). Proton delivery was first postulated as a treatment modality in 1946; however, its clinical efficacy has been recognized only recently (10).

Proton therapy uses the Bragg peak phenomenon to optimize treatment at a specific tissue depth (Fig 1). This is a phenomenon where the proton beam releases most of its energy in the final few millimeters of its range. Techniques such as altering beam energy allow modulation of the depth at which this occurs. With this, radiation dose distal to this point is nearly nonexistent, reducing potential damage to distal radiosensitive structures (11). Despite the improved therapeutic advantage (12), proton therapy is less commonly used secondary to the increased costs associated with construction and operation of the facility (13).

Treatment Planning

Owing to the higher dose per fraction, greater precision and accuracy are required to deliver SBRT safely and effectively (7). To achieve this, the American College of Radiology and American Society for Radiation Oncology (ASTRO) have proposed practice parameters to guide the practical aspects of treatment (7).

A radiation therapy department consisting of qualified staff maintaining appropriate levels of training and expertise is required to safely administer SBRT. The radiation oncologist oversees and approves the treatment with the assistance of qualified dosimetrists, medical physicists, and radiation therapists. SBRT practice should be guided by departmental protocols with reliable quality assurance and control processes (7). Necessary required equipment typically includes a CT/MR simulator, linear accelerator, and in-room image guidance.

Positioning and immobilization are vital to ensure the accuracy and precision required for

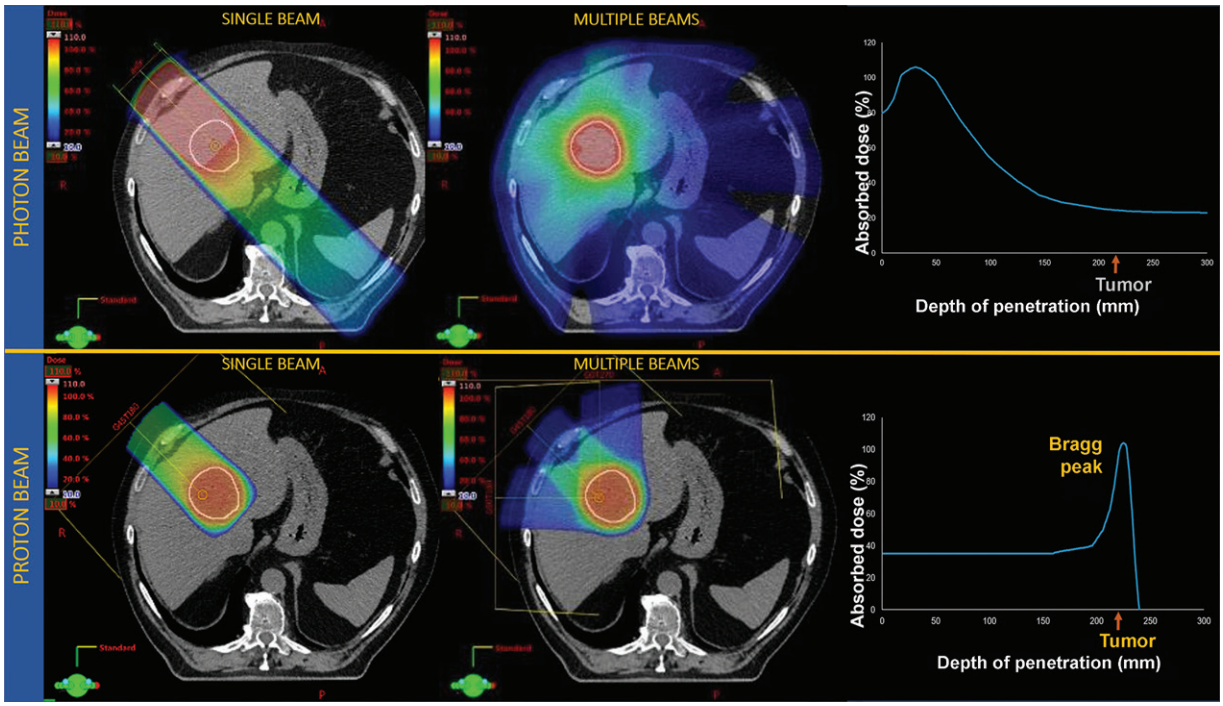

Figure 1. Comparison of photon therapy (top) and proton therapy (bottom) using a single beam and multiple beams. Top graph shows the absorbed dose per depth of tissue; bottom graph shows the Bragg peak associated with proton therapy.

optimal treatment. Proper positioning may be ensured by using a frame-based or frameless system. Frame-based systems use molds to immobilize the patient in the treatment position. External fiducials may be used as reference points to improve localization. Frameless systems use internal fiducial markers in the form of metallic seeds inserted adjacent to the tumor, adjacent bone structures, or the target itself for image guidance. External immobilization aids may also be used in frameless systems, ensuring patient comfort. Motion assessment is often performed with four-dimensional CT with motion-control methods, including abdominal compression, breath holding, respiratory gating, and respiratory tracking.

Treatment planning involves delineation of target volumes and normal organs at risk (OARs) (Fig 2). The ability to perform accurate contouring relies on high-quality planning images in the form of CT, MR, or PET images. The gross tumor volume (GTV) represents the volume of tumor demonstrated at imaging. The clinical target volume (CTV) includes the GTV plus likely subclinical adjacent microscopic disease. The planning target volume (PTV) includes an extra volume beyond the CTV that allows for variations in size, shape, and position of the CTV, including breathing-motion variations. OARs are therefore also identified.

Specific computer systems are then used to optimize treatment plans that deliver the specified dose to the GTV, CTV, and PTV while minimizing the dose to OARs. With photon SBRT, the dose gradually declines outside the PTV, typically asymmetrically and up to several centimeters beyond the PTV boundary. With proton SBRT, the dose drops rapidly outside the PTV owing to the Bragg peak phenomenon (11).

Treatment plans are reviewed and approved by the radiation oncologist. The quality control process must be maintained, with verification of treatment delivery by referring to in-treatment images, often CT. External or internal fiducials may be assessed multiple times or continuously during treatment delivery. Correction strategies may also be required to address any issues with positioning.

Indications and Efficacy

There can be variability in the practice of SBRT between institutions based on available experience and technology (6). The American Society for Radiation Oncology (ASTRO) strongly recommends EBRT as a potential first-line treatment in patients with liver-confined hepatocellular carcinoma (HCC) who are not candidates for curative therapy (14). In our institutional experience, SBRT is reserved for patients with inoperable primary liver cancer (HCC, cholangiocarcinoma) or inoperable metastatic disease, typically in situations not suitable for thermal ablation or intra-arterial embolization. However, other institutions may use it as the primary form of local-regional therapy.

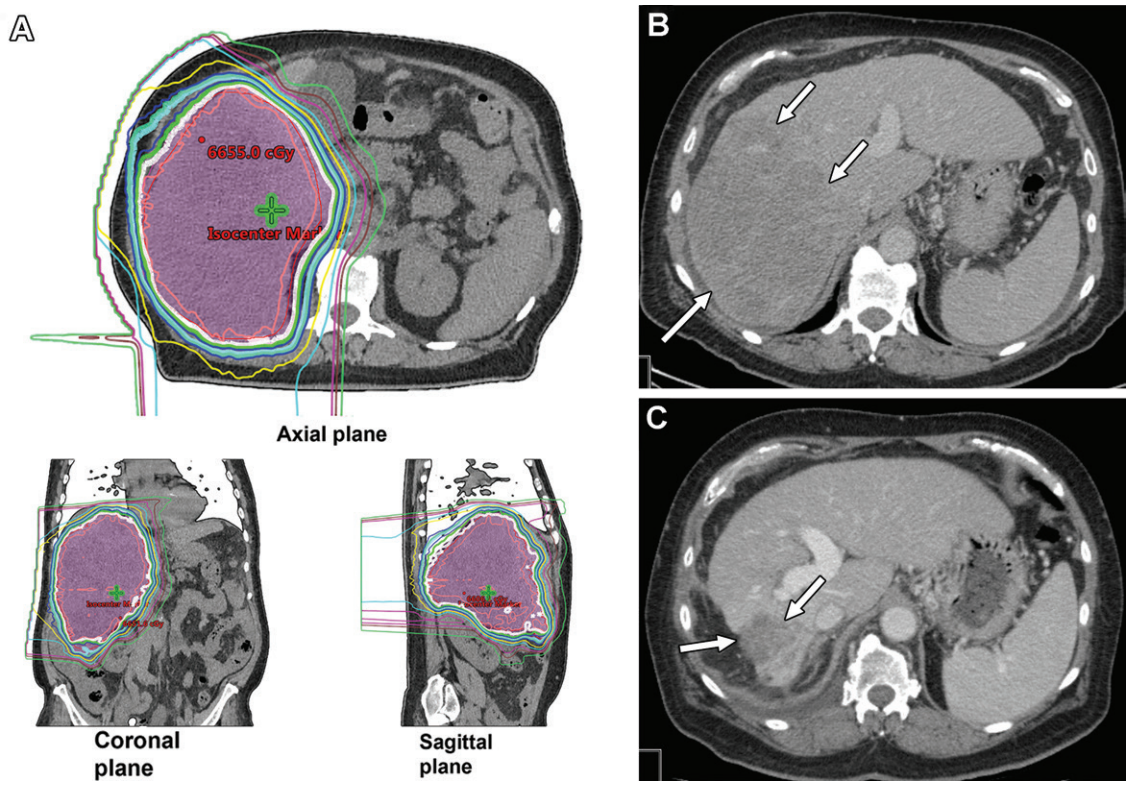

Figure 2. Hepatocellular carcinoma (HCC) in a 75-year-old man. **(A)** CT images from pretreatment SBRT planning show a large radiation field. **(B)** Pre-SBRT axial CT image shows a large HCC (arrows) measuring 101 × 94 mm in the right lobe of the liver. **(C)** Post-SBRT axial CT image shows excellent response of the HCC (arrows) with marked reduction in both enhancement and size, now measuring 43 × 34 mm.

In addition, there is increasing data supporting SBRT as an effective and safe bridging option in patients awaiting liver transplantation (15–17), and this indication is conditionally recommended by ASTRO (14). ASTRO guidelines also strongly recommend EBRT as consolidative therapy after incomplete response to liver-directed therapies and as a salvage option for local recurrences. The data on use of SBRT for multifocal tumors and in the liver for limited large tumors is still evolving. The ASTRO guidelines conditionally recommend use of EBRT in patients with multifocal or unresectable HCC or those with macrovascular invasion and sequenced with system- or catheter-based therapies. In contrast to surgery and other local therapies, SBRT may also be used for treatment of select HCCs with evidence of macrovascular invasion (14).

Safety concerns such as liver functional reserve and tumor position related to other structures are considered on an individual basis. Tumor position as a barrier to treatment is based on local experience and detailed pretreatment planning. Liver functional reserve is typically assessed by means of the patient's Child-Pugh class. Patients with Child-Pugh class A and select patients with Child-Pugh class B are considered eligible for SBRT, with Child-Pugh class B patients more at risk for liver decompensation. The data on use in patients with Child-Pugh class C are limited, and they are considered at high risk for developing RILD even with small doses; therefore, SBRT is to be used with great caution in these patients.

Hepatocellular Carcinoma

The data supporting the efficacy of SBRT in HCC are growing (18–25), as evidenced by the addition of SBRT to the National Comprehensive Cancer Network (NCCN) guidelines as a viable method of treatment of locally advanced HCC. In a large study of 436 HCCs in 297 patients (18), the 1-, 3-, and 5-year overall survival rates after SBRT were 77%, 39%, and 24%, respectively. The rate of local recurrence was low: 13% at 3 years. RILD occurred in 15.9% of patients. Similar results have been observed in other studies (19–25).

Comparative studies suggest that SBRT may be noninferior to radiofrequency ablation (26); however, many of these studies were retrospective evaluations, and no head-to-head prospective comparative studies exist, to our knowledge. However, radiofrequency ablation may be more cost-effective as an initial treatment when compared with SBRT (27,28). Initial studies that compared SBRT with arterially directed therapies demonstrated superior local control and re-

duced hospitalization stay (29,30). When proton SBRT was compared with photon SBRT, proton SBRT appeared to be associated with similar local tumor control, with a potentially lower risk of RILD due to liver-sparing techniques (31).

Although experience with SBRT in HCC is increasing and encouraging as an alternative local-regional treatment, it is not widely available and data from a large cohort are still lacking. Therefore, it is not yet formally adopted by well-known treatment guidelines in HCC, such as the Barcelona Clinic Liver Cancer (BCLC) guidelines.

Intrahepatic Cholangiocarcinoma

There are limited data supporting SBRT in treatment of intrahepatic cholangiocarcinoma (ICC). In a study of 39 patients treated with SBRT for inoperable ICC, the local control rate at 2 years was 94%, with an overall survival rate at 2 years of 47% (24). Similar results were described in a retrospective study of 66 patients with ICC, which demonstrated a 2-year local control rate of 93% and an overall survival rate of 62% (32). Despite the absence of high-quality long-term data, SBRT is considered an efficacious and safe modality for treatment of inoperable cholangiocarcinoma.

Liver Metastases

Along with surgery and ablation, SBRT can play a role in treatment of select patients with liver metastases, with the choice for local therapy dependent on institutional expertise and patient and tumor characteristics (33). A recent single-institution retrospective review of 150 liver metastases (from a variety of primary sites) that received radiation therapy showed a mean overall survival rate of 20.4 months and a median local control rate of 35.1 months (34). Nine percent of patients developed a significant toxic effect.

In another study, long-term follow-up of 76 cases of colorectal cancer with metastases only in the liver in a phase II trial demonstrated a 5-year local control rate of 78% with an 18% overall survival rate (35). In this study, a more favorable local control rate was demonstrated with breast, gynecologic, and colorectal primary sites. There were no cases of RILD, with only one patient experiencing a significant toxic effect.

These studies confirm the role of SBRT as a viable form of local-regional therapy for liver malignancy in the appropriate clinical setting.

Mechanisms of Radiation Treatment Effects

Physiologic Mechanism

The biologic processes that underpin the efficacy of SBRT are not completely understood. It is generally accepted that there are direct and indirect mechanisms of cell death after irradiation. There is ongoing debate with regard to the level of contribution from each mechanism. The direct mechanism of cell death occurs secondary to double-stranded breaks in DNA and results in cell death. Indirect mechanisms are believed to arise from vascular damage and antitumor immune response, in which the tumor cells remain metabolically active after treatment until eventual cell death (36).

Tumor vessels are often structurally abnormal, with irregular endothelial cells interspersed around tumor cells and an incomplete basement membrane with disorganized pericytes (36). This results in functionally abnormal vessels compared with those of adjacent normal tissue. After EBRT, it has been proposed that direct damage to endothelial cells (37) and compression of small vessels (38) lead to vascular compromise of the tumor. In contrast, the vascularity of normal tissue is more robust, with a strong inflammatory reaction and vasodilatation initially followed by progressive changes occurring more slowly, over months to years (36). Ischemic changes in normal tissue progress over this time, secondary to fibrotic obliteration of associated blood vessels; this is thought of as the primary mechanism for development of radiation-induced late normal tissue effects (Fig 3). This occurs in a dose-dependent manner (39–42).

High-dose EBRT has demonstrated an ability to promote antitumor immunity (43,44). In effect, the death of multiple tumor cells results in increased circulating immune-modulating proteins and increased transit of tumor-specific T cells to the tumor (45,46). Also, in combination with immunotherapy, these effects may be upregulated and result in greater efficacy to inhibit the development of metastases (36,44). The degree to which this immune response results in a clinically effective response has not been clinically ascertained, and treatment considerations should not be based on this potential phenomenon.

SBRT may cause cell dysfunction or death in adjacent normal tissues. The radiosensitivity of cells and tissues can be quite heterogeneous. Often, sublethal damage may result in enough dysfunction to result in progressive changes over a longer period (36). Tissues are typically classified as *(a)* functioning in series (eg, spinal cord, stomach, or intestine), in which a high dose of radiation to even a small volume can cause severe injury, or *(b)* functioning in parallel (eg, liver parenchyma or kidneys), in which a larger volume of tissue receiving even a low dose of radiation can cause severe injury.

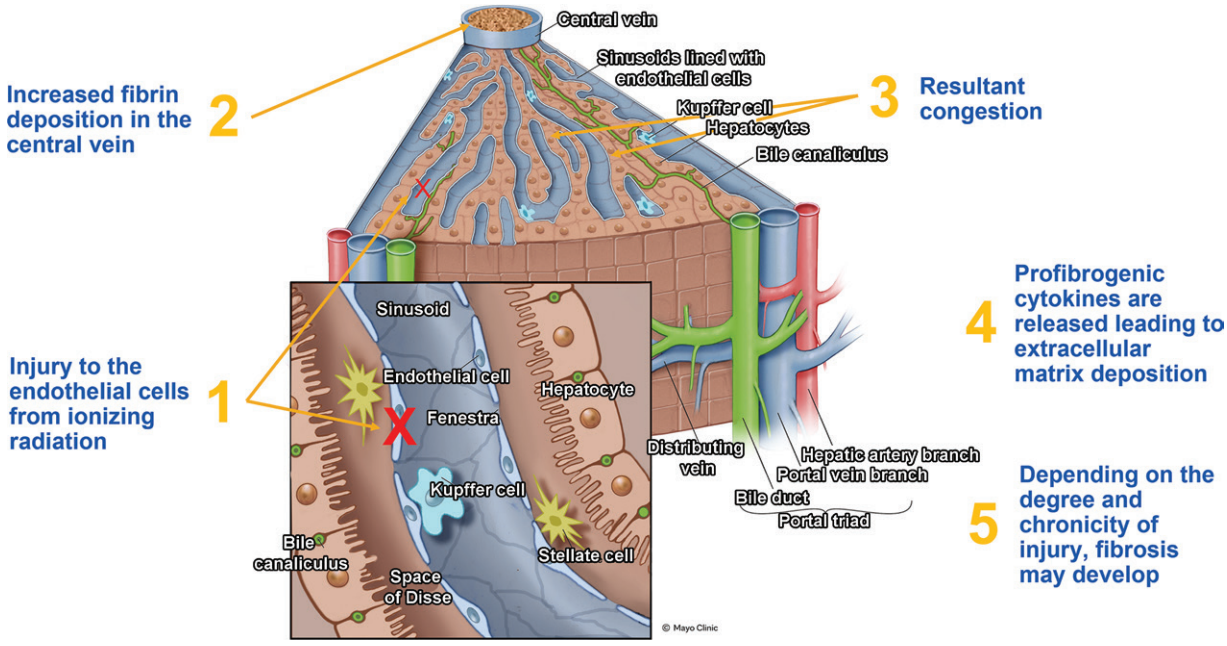

Figure 3. Parenchymal changes after SBRT. Endothelial cells lining the liver sinusoids are very sensitive to radiation injury *(1)* after SBRT, leading to fibrin deposition in the sinusoids and ultimately collagen deposition in the central veins *(2)*. The fibrosis or occlusion of the central vein results in congestion of the hepatic sinusoids *(3)*. If the insult persists, other cellular mechanisms are activated, leading to deposition of extracellular matrix *(4)*, and eventually fibrosis develops *(5)*.

Pathologic Findings

The pathologic changes identified are predominantly the sequelae of direct cell death or vascular interruption to the tumor and surrounding liver. With positive treatment effect, the tumor demonstrates coagulative necrosis and fibrosis, as identified by its tan color at gross examination. This is surrounded by the discolored and congested hepatic parenchyma (Fig 4).

Endothelial cells lining the sinusoids and vessels are very radiosensitive, and radiation injury leads to activation of soluble clotting mechanism (47). Histologically, fibrin from endothelial injury is deposited in sinusoids and central veins, leading to thrombosis and progressive vascular occlusion with upstream congestion of the sinusoids (48). A dynamic fibrotic process results in replacement of the fibrin with collagen, ultimately leading to fibrosis and occlusion of the central veins. The hepatocellular plate is often atrophied, with possible thrombosis of the intermediate-sized portal veins. This results in well-demarcated zones of progressive damage, extending from the central area of necrotic tissue to an area of dense fibrosis to a rim of congested hepatic tissue histologically similar to veno-occlusive disease and finally to normal hepatic tissue (Fig 5) (49).

It is important to understand that cancer cells do not die immediately after irradiation. Radiation-induced damage leads to cell death by *(a)* mitosis-linked death, whereby a cell passes through mitosis and dies owing to unrepaired DNA breaks and chromosomal aberrations (50); *(b)* apoptosis, which is programmed cell death; and *(c)* radiation-induced senescence, in which cells remain metabolically active but incapable of division (50). After radiation injury to DNA, tumor cells cannot grow or divide anymore; however, the effect is not immediate on the resting stage cells or those that are dividing less often (50).

Therefore, it may take several days, weeks, or months for cancer cells to start dying, a process that could take months after treatment ends. As a result, tumor may be viable for weeks to months after SBRT and not shrink for this period. This in combination with maintained tumor vascularity until complete tumor necrosis can confound imaging assessment of treatment response.

Imaging Findings

Tumor Changes

There are emerging data regarding the imaging features of hepatic tumors after SBRT. Most of these data are from retrospective imaging reviews, the majority of which lack explant data.

Imaging after SBRT is usually performed with multiphasic contrast-enhanced MRI or CT every 3 months after treatment. Imaging characteristics used to evaluate tumor response include changes in enhancement or size of the treated lesion at multiphasic cross-sectional imaging (Figs 6, 7). It is important to note that the changes in tumor size or enhancement after SBRT may take months to manifest at imaging; therefore, images obtained sooner than at least 3 months after

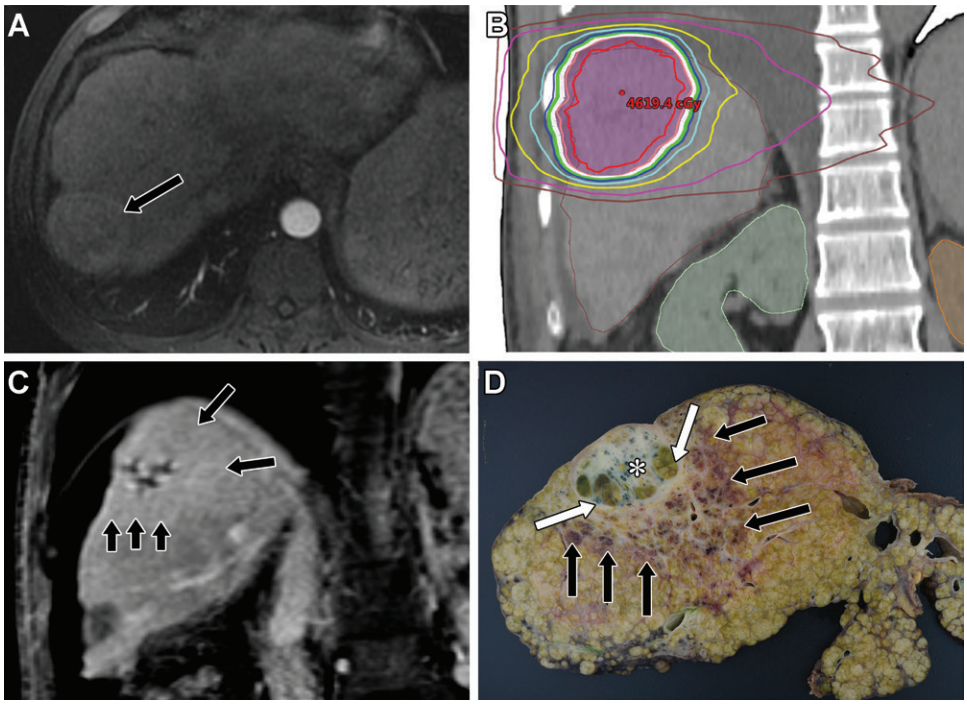

Figure 4. HCC in a 53-year-old man with chronic liver disease. **(A)** Axial contrast-enhanced T1-weighted image shows a 36 × 39-mm enhancing lesion (arrow) in the right hepatic lobe. **(B)** Coronal CT image shows the SBRT planning. **(C)** Coronal late arterial phase gadolinium-enhanced T1-weighted image 6 months after SBRT shows persistent internal enhancement within the HCC and a peripheral geographic area of enhancement (arrows), correlating with the irradiated liver volume and consistent with focal liver reaction (FLR). The patient underwent orthotopic liver transplant after 10 months. **(D)** Photograph of the cut section of the explant native liver shows necrotic tumor (*) with a surrounding rim of fibrosis that appears tan (white arrows) and an area of congested liver (black arrows), which correlates with the FLR at imaging and appears dark red.

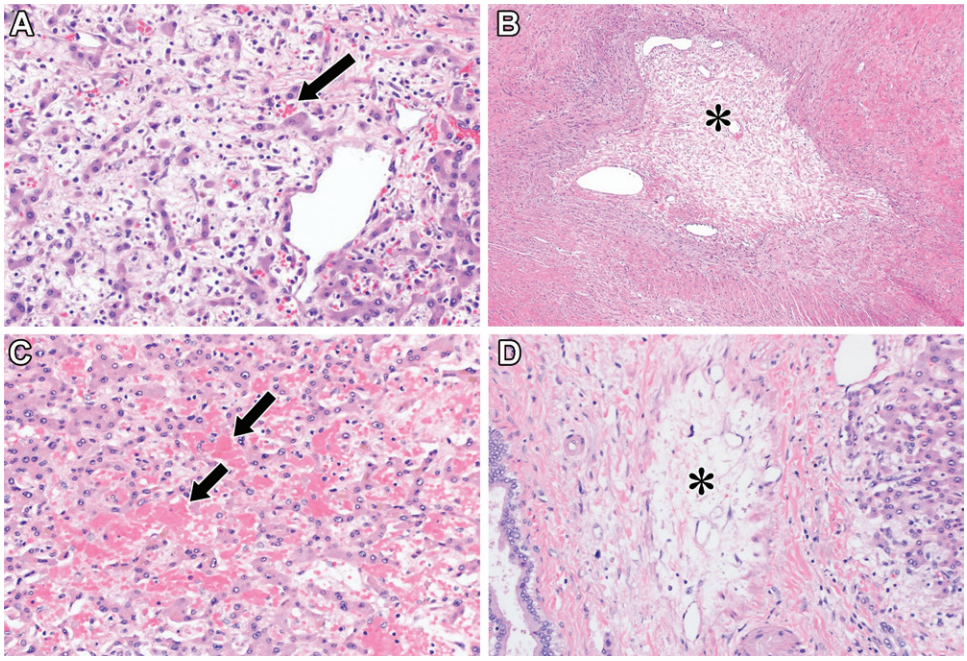

Figure 5. Pathologic changes in the liver parenchyma after SBRT. (Hematoxylin-eosin stain, varying original magnification.) **(A)** Photomicrograph shows parenchymal collapse with loss of hepatocytes and accumulation of scattered pigmented macrophages (arrow). **(B)** Photomicrograph shows obliteration of the central vein (*) with associated collagen deposition. **(C)** Photomicrograph shows resultant dilatation and congestion of the sinusoids (arrows), which contain red blood cells. Atrophy of the hepatocellular plate is frequent. **(D)** Photomicrograph shows thrombosis of intermediate-sized portal veins (*), which is also sometimes seen.

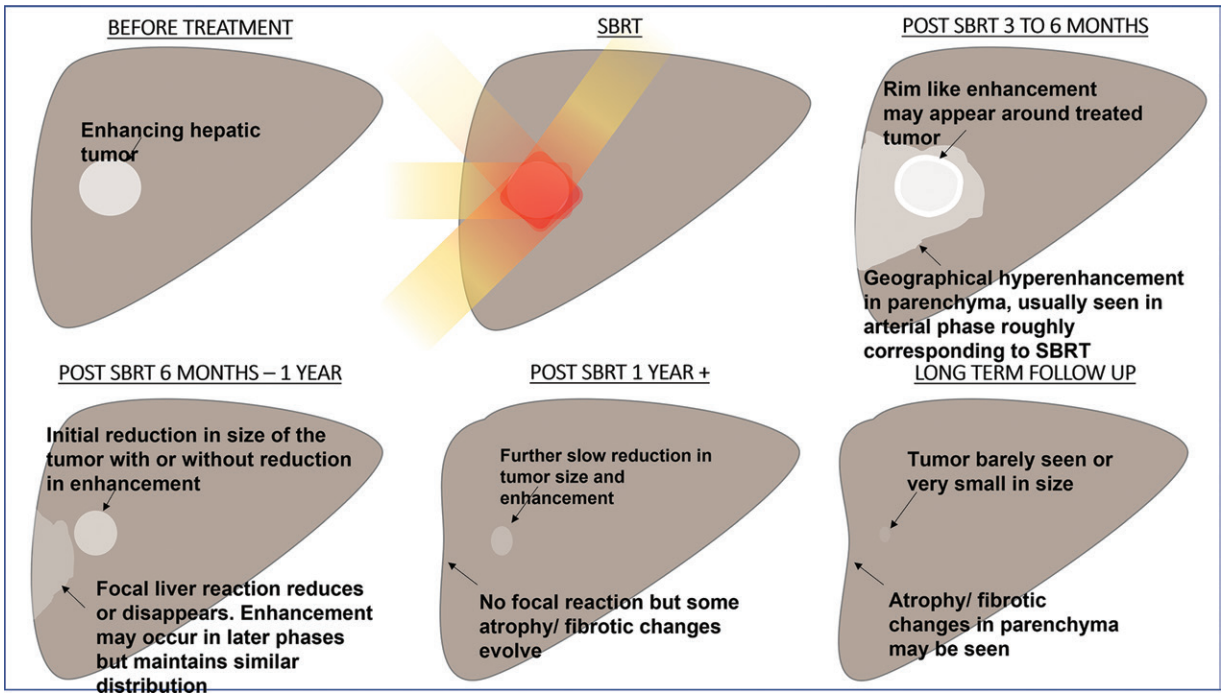

Figure 6. Diagram shows expected changes after SBRT.

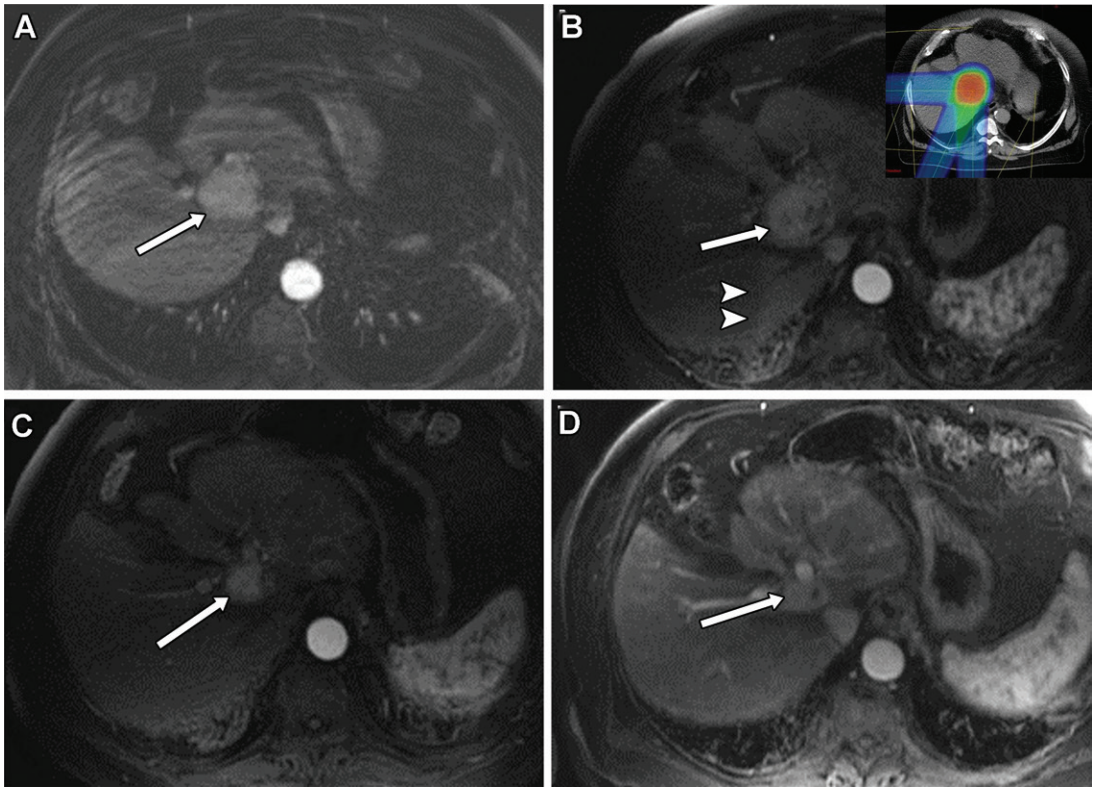

Figure 7. New diagnosis of HCC in a 65-year-old patient. The tumor was considered unresectable owing to its proximity to the hepatic veins and hilum. The patient underwent SBRT. Late arterial phase T1-weighted images before SBRT **(A)** and 6 **(B)**, 12 **(C)**, and 16 **(D)** months after SBRT show the lesion (arrow). The post-SBRT images show progressive decrease in size and enhancement from 47 mm in greatest dimension before SBRT to 24 mm at 16 months. Note the geographic area of hyperenhancement (arrowheads in **B**) at 6 months, which correlates with the area of the liver that received greater than 30 Gy of radiation. (Inset in **B**: Image shows proton SBRT planning.)

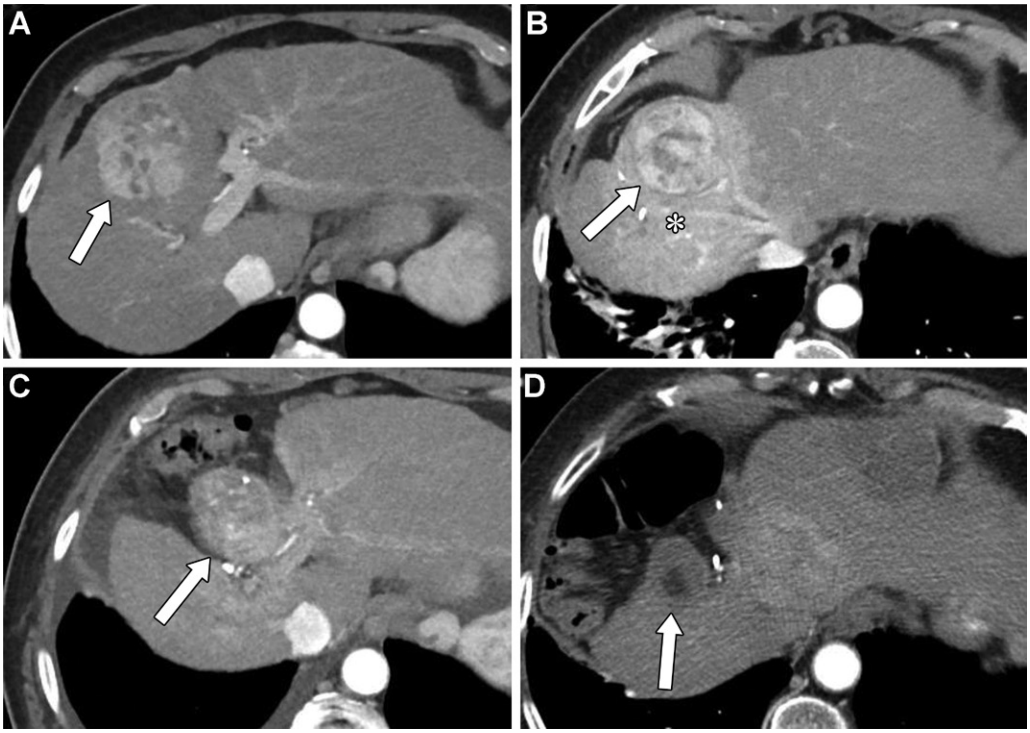

Figure 8. Temporal evolution of post-SBRT changes in the treated tumor in a 66-year-old man. **(A)** Axial late arterial phase CT image before SBRT shows a Liver Imaging Reporting and Data System (LI-RADS) LR-5 observation (arrow), compatible with HCC. The LR-5 observation is in the right hepatic lobe and measures 48 × 40 mm. **(B)** Axial late arterial phase CT image 6 months after SBRT shows persistent enhancement of the lesion (arrow) with no significant change in size. Note the geographic peritumor hyperenhancement (*), which represents focal liver reaction (FLR) to radiation. **(C)** Axial late arterial phase CT image 1 year after SBRT shows decreasing enhancement of the lesion (arrow) and decrease in size to 40 × 31 mm. Note the accompanying progressive atrophy of the right hepatic lobe. The arterial enhancement of the lesion persisted at follow-up CT at 15 months (not shown), with increase in size consistent with progression, which required rescue embolization for control of disease. **(D)** Axial late arterial phase CT image 2 years after SBRT and 6 months after embolization shows persistent but decreased enhancement of the tumor (arrow), which is isoenhancing to the liver with a central area of necrosis and decreased size, now measuring 32 × 25 mm.

irradiation should be interpreted with caution for evaluation of treatment response and local progression (49). Additionally, SBRT may cause an inflammatory response in both the targeted tumor and surrounding hepatic parenchyma in the early posttreatment period.

Hepatic tumor size reduction after SBRT is variable, with retrospective data showing a wide range in expected treatment response times (Fig 8). Studies that evaluated SBRT-treated HCC showed that volume reduction at 3 months can vary from 24% to 60% (51–53). Another study showed that volume reduction at 3, 6, 9, and 12 months was 35%, 37%, 48%, and 55%, respectively (51). Similar results were seen after SBRT of hepatic metastases (52,54) and cholangiocarcinoma; however, data are limited (52). After SBRT, an increase in tumor volume—outside of the immediate posttreatment period—suggests local tumor progression (55). Therefore, assessment of tumor size in grading response in the first 6–12 months demonstrates poor accuracy, often related to persistent viable tumor and necrosis, given the pathophysiology of radiation-induced cell death.

Treatment response assessment using enhancement as an imaging biomarker has been proposed as a measure of response (51). Multiple studies have shown that there is persistent enhancement in HCC treated with SBRT, which can persist for up to and longer than 1 year (51,55–57). Up to 75% of successfully treated HCCs demonstrate persistent arterial phase hyperenhancement (APHE) up to 6 months after therapy (55). However, the majority of successfully treated HCCs demonstrate loss of enhancement after SBRT within the 1st year (51,57), with one study suggesting a mean duration of 5.9 months for loss of enhancement in SBRT-treated HCC (53).

Brook et al (52) showed an increase in the area of the nonenhancing portions of hepatic tumors after SBRT, from 27% before therapy to 59% after therapy in HCCs and from 20% to 61% in metastases. In a study on the post-SBRT appearance of HCC, Price et al (51) showed that the percentage of necrosis (nonenhancement) was

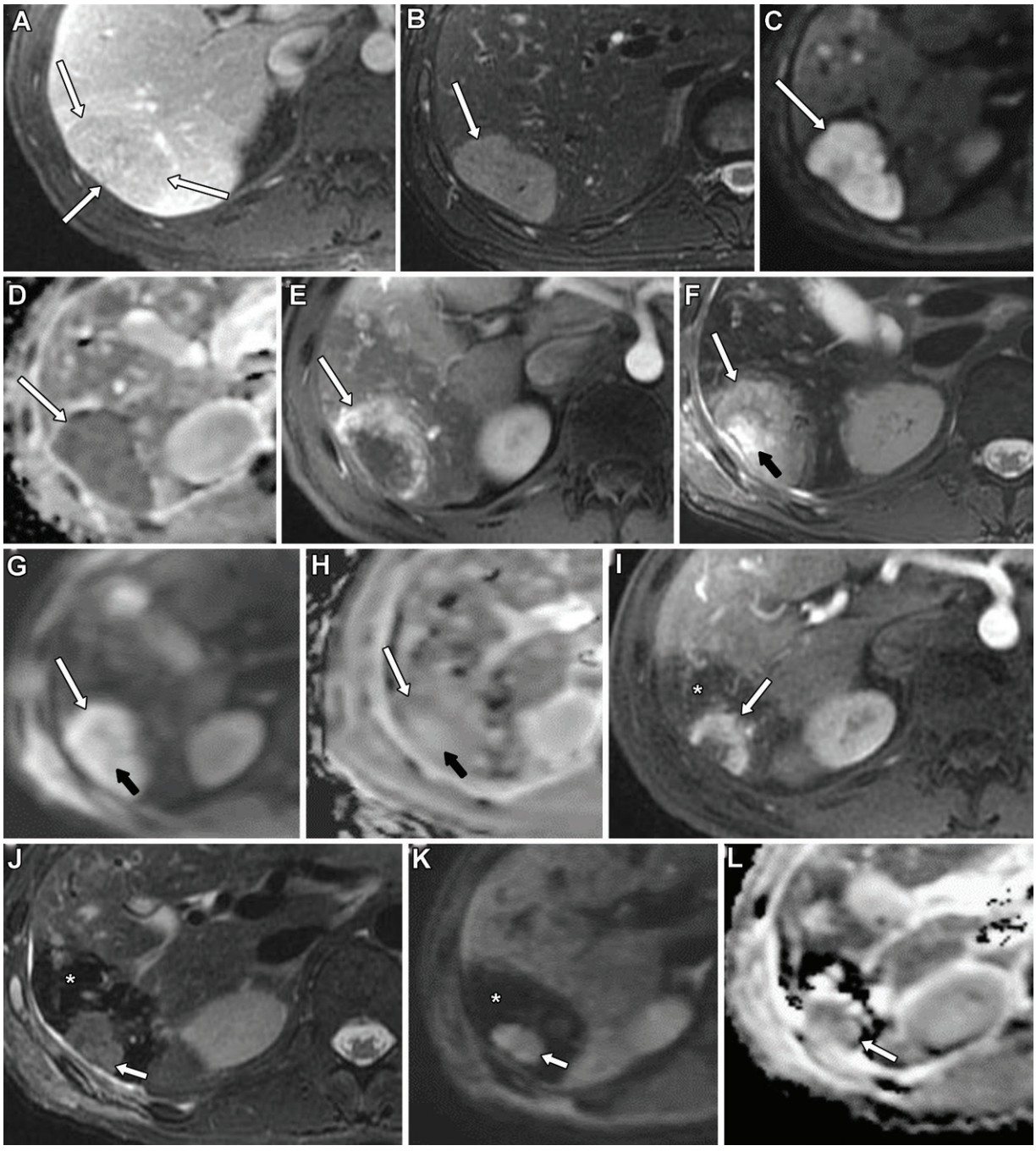

Figure 9. Metastasis from medullary thyroid cancer in a 48-year-old woman. Axial MR images before SBRT **(A–D)**, 6 months after SBRT **(E–H)**, and 1 year after SBRT **(I–L)** show the metastasis (white arrows). The metastasis measured 31 × 54 mm before SBRT; at 6 months, it shows a mild decrease in size, measuring 29 × 52 mm; at 1 year, its size decreases further to 24 × 35 mm. Contrast-enhanced late arterial phase T1-weighted images **(A, E, I)**, T2-weighted images **(B, F, J)**, diffusion-weighted images **(C, G, K)**, and apparent diffusion coefficient (ADC) maps **(D, H, L)** were obtained. The original enhancement of the metastasis **(A)** decreases at 6 months **(E)**; however, some enhancement persists at 1 year **(I)**. At 6 months, there is a central area of T2 hyperintensity (black arrow in **F**), with decreased signal intensity on the diffusion-weighted image (black arrow in **G**) and increased signal intensity on the ADC map (black arrow in **H**), suggestive of tumor necrosis. At 1 year, the necrosis decreases further in size, with decreased signal intensity on the diffusion-weighted image **(K)** and increased signal intensity on the ADC map **(L)**. At 1 year, the T1-weighted **(I)**, T2-weighted **(J)**, and diffusion-weighted **(K)** images show a thick hypointense rim (*), which likely represents hemosiderin deposition, thought to be secondary to congestive changes in the liver parenchyma surrounding the treated tumor.

greater than the percentage reduction in tumor size at each time point of follow-up. Although reduced enhancement is historically a biomarker of response in hepatic tumors, SBRT-treated liver malignancies often show persistent enhancement in the early posttreatment phase (Figs 8, 9), which can last up to and beyond 1 year and should not be mistaken for viable tumor that needs treatment. These cases should be assessed in their entirety, referencing other imaging biomarkers and serial

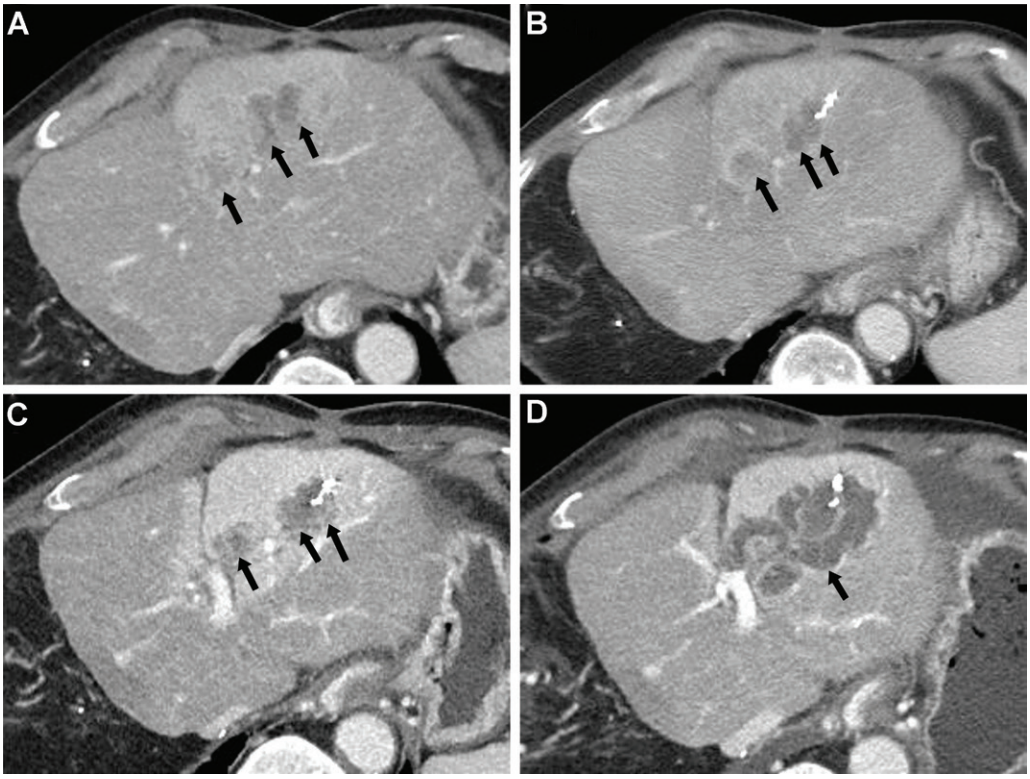

Figure 10. Recurrent metastases from colorectal cancer in a 74-year-old man. The metastases were previously treated with right hepatectomy and wedge resections in the left lobe. **(A)** Axial CT image shows biopsy-proven recurrence in the left lobe (arrows), which manifests as two hypoenhancing lesions. The lesions were treated with proton-beam SBRT. **(B)** Axial CT image 3 months after SBRT shows that the metastases remain stable to mildly decreased in size, with a decrease in enhancement. **(C, D)** Axial CT images at 6 months **(C)** and 9 months **(D)** show that the nodules (arrows) have increased in size, indicating disease progression.

assessment over time—including multidisciplinary discussion—to reach a conclusion on treatment response.

In addition to CT or MRI, PET has been shown to be useful in evaluation of treatment response after SBRT, particularly in cases of cholangiocarcinoma or liver metastases. HCC has variable presence of intracellular glucose-6-phosphatase enzyme, resulting in low sensitivity of 36%–55% for identification of HCC with PET (58,59). The degree of fluorodeoxyglucose (FDG) avidity is greater in poorly differentiated HCC (59). Assessment of FDG activity at PET/CT may provide a potential biomarker, particularly in cases of metastatic disease. Indeed, complete metabolic response at FDG PET/CT has been demonstrated to appear before anatomic measures of response were evident (Fig E1) (60).

In one study of metastatic lesions that ultimately demonstrated lesion control, maximum standardized uptake value (SUV_{max}) decreased by half at 2 months and reached a plateau SUV_{max} of 3.1 at 5 months (61). Local control was defined as SUV_{max} less than 6 and no progression using Response Evaluation Criteria in Solid Tumors (RECIST). In this study, the SUV_{max} of lesions was found to fluctuate to 4.2 even in lesions where control was attained. Therefore, a cutoff SUV_{max} of 6 was proposed to define failure when SUV_{max} had previously been below 6 (54).

Although demonstrating poor sensitivity in diagnosis of HCC, FDG PET/CT may aid in assessing for response after SBRT in FDG-avid lesions. In a retrospective review of 31 patients, a cutoff tumor SUV_{max} of 3.2 demonstrated a 4-year control rate of 86% (62). Median follow-up time was 18 months in this study.

Other imaging biomarkers may also provide ancillary information in assessment of tumor response, particularly T2 signal intensity and apparent diffusion coefficient (ADC) at MRI. Typically, tumors demonstrate a decrease in T2 signal intensity and an increase in ADC after treatment (Fig 9). An increase of 20% or greater in ADC was found to be significant in assessing the response of HCC in one study (63), with an increase of 25% identified as a predictor of in-field response of HCC (64).

Local tumor progression is typically defined as increase in size on more than one serial study over time, or new or increased enhancement of the treated tumor (Fig 10) (48). Increased SUV_{max} greater than 6 or persistence of FDG

Table 1: Imaging Changes in Adjacent Liver Parenchyma after SBRT

Type of Changes by Time after SBRT	Pathologic Changes	Imaging Findings
Acute (1–3 months)	Sinusoidal congestion Perisinusoidal hemorrhage Hepatocyte apoptosis and degeneration	Hypoattenuation or hypointensity surrounding tumor Arterial hyperenhancement with or without portal venous hyperenhancement With or without rim enhancement
Subacute (3–6 months)	Plus occlusion of sublobular veins	Hypoenhancement in portal venous phase Hyperenhancement in delayed phase With or without rim enhancement
Chronic (>6 months)	Fibrosis or occlusion of central veins Distortion of lobules Kuppfer cell accumulation with or without hemosiderin	Enhancement characteristics may normalize Hypointensity may persist owing to hemosiderin Atrophy and volume loss

activity above background over two serial PET/CT studies is also predictive of recurrence or treatment failure (60).

Specific Measures of Response

There are many treatment response assessment systems used to characterize tumor response after treatment. The most commonly used for liver tumors are RECIST, modified RECIST (mRECIST), and the Liver Imaging Reporting and Data System (LI-RADS). RECIST uses data based on size alone, whereas mRECIST and LI-RADS use tumor enhancement for treatment response assessment.

There are limited data on the efficacy of these algorithms after SBRT therapy. A recent retrospective review of 40 HCCs treated with SBRT that ultimately underwent explantation did demonstrate that LI-RADS performs well in predicting complete and incomplete necrosis (65). When the LI-RADS treatment response (LR-TR) equivocal category was considered as nonviable, sensitivity and specificity were 71%–86% and 85%–96%, respectively.

However, the limitations of these algorithms are self-evident when the imaging features outlined earlier are considered. Relying on dimensional data alone would not allow evaluation of treatment effect, given the slow tumor shrinkage immediately after SBRT. Also, as evident in recent studies that assessed the enhancement characteristics of HCC after SBRT, the presence of APHE is common, especially in the first 12 months after SBRT; thus, using mRECIST and LI-RADS to assess treatment response could be flawed, given that APHE is expected. Thus, a multidisciplinary approach to evaluation of SBRT-treated tumors by assessing multiple considerations—including imaging features, laboratory values, and clinical factors—is often necessary to appropriately manage these patients.

Parenchymal Changes

In the first few months after SBRT, congestive and edematous changes in the hepatic parenchyma combined with cell death and physiologic healing response by the liver can be described as focal liver reaction (FLR) (66). Imaging features are seen initially approximately 1 month after treatment and then peak at 3–6 months (67). The degree of FLR depends on the radiation dose received, prior local treatment, and extent of underlying liver dysfunction. It can be further divided into three phases: acute, subacute, and chronic (Table 1) (48).

At noncontrast CT, FLR in the acute phase (1–3 months) manifests as a geographic area of hypoattenuation in the radiation field on noncontrast images, which generally enhances greater than surrounding tissue in the contrast-enhanced arterial phase (Figs 7, 8, 11) (68). This is due to inflammatory response in the parenchyma and may lead to erroneous assessment of lesion progression. There may be relative hypoenhancement of the affected area in the portal venous phase, as congested vessels would receive delayed or less iodinated contrast material secondary to increased sinusoidal pressures (48). The FLR demonstrates relative T1 hypointensity and T2 hyperintensity at MRI, likely due to edema. The FLR demonstrates hyperintensity on diffusion-weighted images and also hyperintensity on ADC maps, presumably from T2 shine-through and edema (69).

In the subacute phase (3–6 months), hypoenhancement in the portal venous phase persists with possible increased delayed enhancement secondary to impaired clearance of contrast material (70). Rarely, rimlike enhancement around

Figure 11. FLR in a patient with hepatitis C virus–related cirrhosis and hepatocellular cancer. **(A)** Axial late arterial phase contrast-enhanced MR image shows the hepatocellular cancer (arrow). **(B)** Corresponding MR image 3 months after SBRT shows acute FLR (arrows), which is characterized by APHE on late arterial phase images. **(C, D)** Corresponding portal venous phase **(C)** and delayed phase **(D)** images show that the FLR persists (arrows) and becomes isoenhancing to mildly hyperenhancing. This finding is important to understand, as locally progressive recurrent or infiltrative HCC would likely demonstrate APHE on arterial phase images with washout on portal venous and delayed phase images.

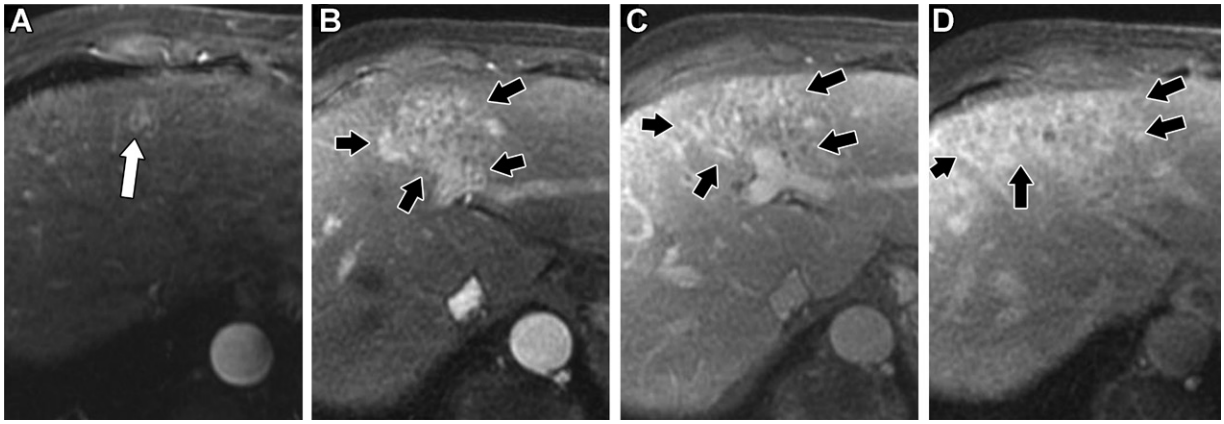

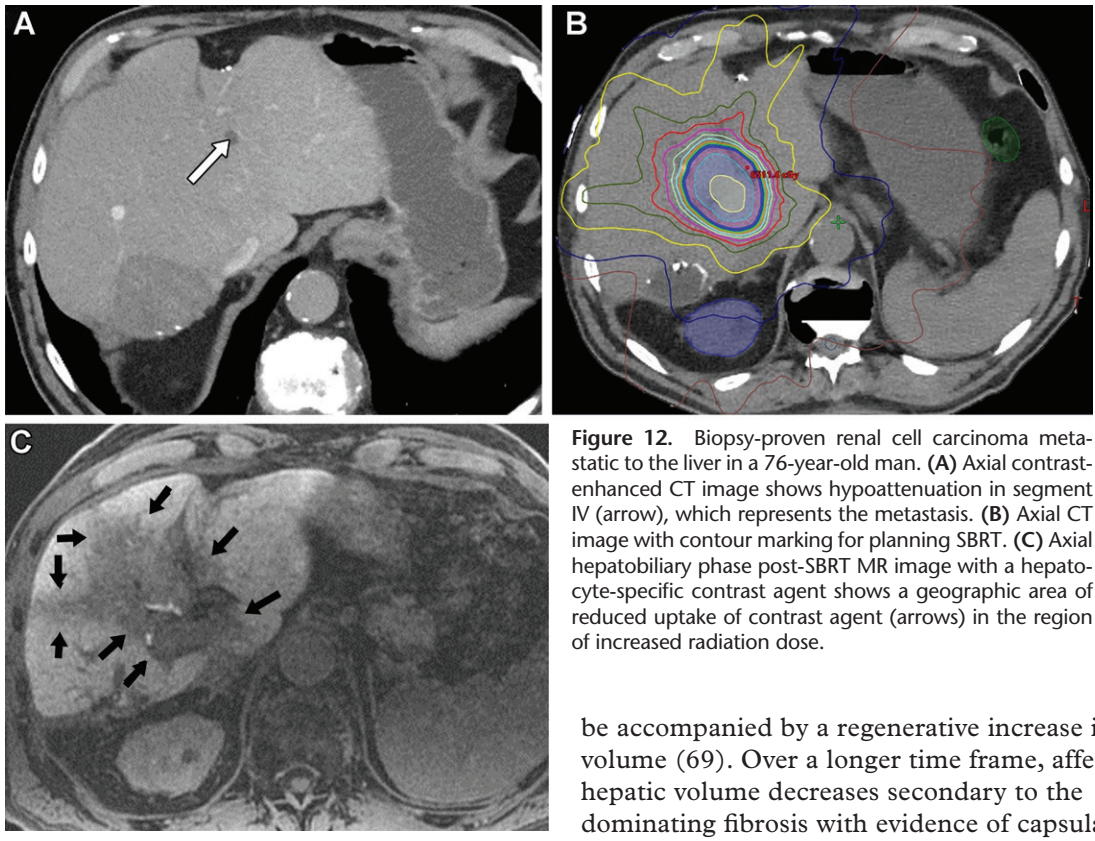

Figure 12. Biopsy-proven renal cell carcinoma metastatic to the liver in a 76-year-old man. **(A)** Axial contrast-enhanced CT image shows hypoattenuation in segment IV (arrow), which represents the metastasis. **(B)** Axial CT image with contour marking for planning SBRT. **(C)** Axial hepatobiliary phase post-SBRT MR image with a hepatocyte-specific contrast agent shows a geographic area of reduced uptake of contrast agent (arrows) in the region of increased radiation dose.

the treated tumor may be visualized in both the arterial and portal venous phases; the exact mechanism is not known but may represent a persistent thin rim of FLR.

The imaging appearance of FLR in the chronic phase (>6 months) is dominated by an underlying dynamic fibrotic process in the hepatic parenchyma. In the first 3 months, the affected liver parenchyma shows progressive decrease in volume. However, this may rarely be accompanied by a regenerative increase in volume (69). Over a longer time frame, affected hepatic volume decreases secondary to the dominating fibrosis with evidence of capsular retraction.

Delayed enhancement is usually seen in the region of fibrosis. If hepatic steatosis is present in the nonaffected liver parenchyma, the affected area may demonstrate fatty sparing secondary to loss of intracellular fat in the hepatocytes (69). Areas of reduced T2 signal intensity may become evident, consistent with hemosiderin deposition (Fig 9) (48). Use of a hepatocyte-specific contrast agent often demonstrates decreased hepatobiliary phase uptake in the area of the liver affected by FLR and the radiation field (Fig 12) (71).

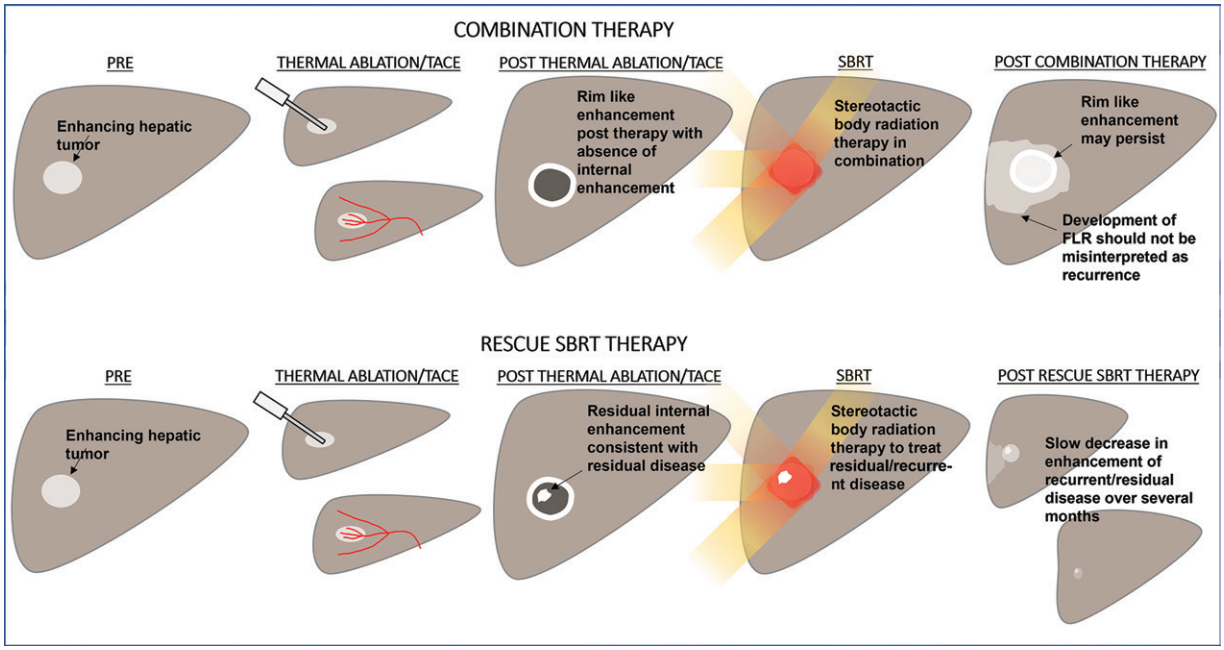

Figure 13. Diagram shows imaging features after treatment with combination therapy (top) and imaging features after SBRT as a rescue therapy (bottom). *TACE* = transarterial chemoembolization.

Imaging Pitfalls

Focal Liver Reaction

The phenomenon of FLR in the acute and subacute phases may complicate assessment and result in misinterpretation of growth in the lesion (Figs 11, E2). The area of reactive hyperemia evident as APHE can be confused with local progression or infiltrative tumor. Close review of the radiation planning images and pretreatment images is useful to understand the radiation field, which should correlate with the imaging appearance of FLR.

In addition, an understanding of the underlying pathophysiology is beneficial. Other imaging features such as absence of mass effect and absence of abnormal restricted diffusion may also be beneficial. Finally, the FLR should resolve or decrease in subsequent imaging studies.

Peripheral Rim Enhancement

As stated earlier, rim enhancement is an uncommon finding after SBRT, predominantly seen after treatment of metastases. However, it may complicate assessment of tumor response (Fig E3), with differentiation from recurrence difficult. Assessment of the radiation field is important to ensure correlation with this region.

Assessment of diffusion restriction and ADC maps may also be beneficial, as residual tumor would demonstrate more marked abnormal diffusion restriction and hypointensity on ADC maps. Assessing the entire clinical picture with assessment of tumor markers (when levels are elevated at baseline) may also aid in clarification. Ultimately, follow-up may show resolution; however, the time frame for resolution of rim enhancement is not definitively outlined (44).

Artifact from Fiducial Markers

Radiation planning and delivery often use placement of fiducial markers to allow adequate colocalization of the tumor target. These are metallic seeds, typically placed percutaneously within 5 cm of the target tumor. However, the fiducial markers can produce streak artifacts obscuring CT images and result in a nondiagnostic study (Fig E4).

The degree of artifact is related to the size and composition of the fiducial markers, with larger and higher-Z materials producing greater artifact. MRI and PET/CT are practical alternative imaging modalities, as these techniques are less affected by the metallic artifact.

Assessment of Response after Combination Therapy

Management of hepatic tumors is often complex, with multiple different treatment algorithms possible, depending on the clinical course. SBRT may be used after other local-regional therapies or as part of a combination approach. For instance, in management of HCC, SBRT is often performed after intra-arterial embolic therapy. Intra-arterial therapy will potentially shrink the tumor, reducing the radiation field of the subsequent SBRT. Intra-arterial therapy such as transarterial chemoembolization (TACE) may also radiosensitize the tumor (72).

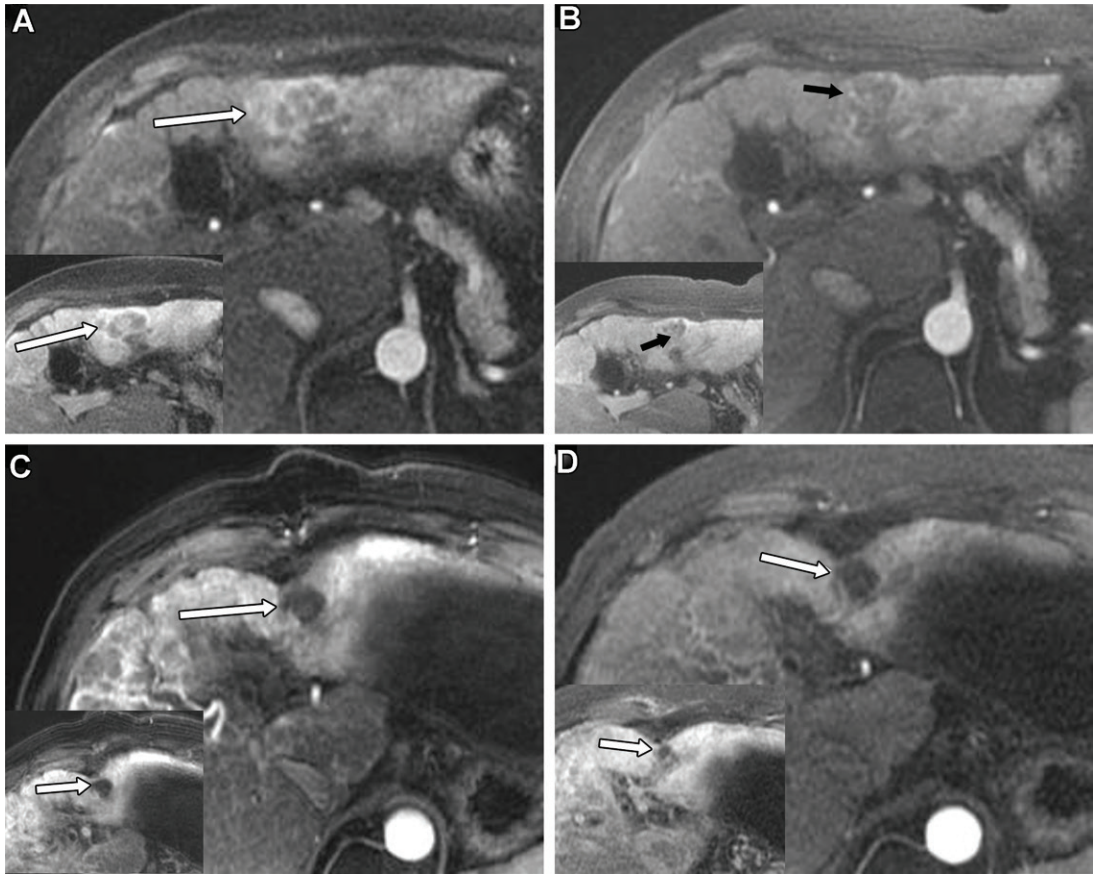

Figure 14. Hepatitis C cirrhosis and HCC in a 70-year-old man treated with transarterial chemoembolization (TACE) followed by SBRT. **(A)** Axial contrast-enhanced MR image shows the HCC (arrow) in the arterial phase and in the portal venous phase (inset). The tumor measures 41 × 28 mm. **(B)** Corresponding image 1 month after TACE shows persistent enhancement within the tumor (arrow) in the late arterial phase and in the portal venous phase (inset), compatible with LI-RADS treatment response (LR-TR) viable disease. The patient was then treated with SBRT. **(C, D)** Corresponding CT images 1 month **(C)** and 3 months **(D)** after SBRT show excellent tumor response, with complete nonenhancement of the treated tumor (arrow) with internal necrosis and decreasing size, now measuring 21 × 19 mm. Extensive FLR with atrophy of the liver is noted after SBRT. In this case, loss of enhancement of the tumor after SBRT allows easier assessment of treatment response than in HCCs, which are treated with SBRT alone only when persistent APHE is identified for several months.

Therefore, assessment of response is often complicated by the preceding ablative procedure or intra-arterial therapy (Figs 13, 14). This is important in ascribing measures of response using algorithms such as LI-RADS (73).

After TACE or thermal ablation, the residual tumor often demonstrates absence of internal enhancement with residual peripheral enhancement (74,75). If SBRT is performed as part of combination treatment or for residual tumor, the subsequent imaging features should adopt typical post-SBRT changes. For instance, FLR should not be misinterpreted as tumor progression. Also, in cases of combination therapy, residual internal nodular enhancement—which may be considered LI-RADS treatment response (LR-TR) viable after TACE alone—may demonstrate typical slow reduction in enhancement over 1 year after SBRT (57,73).

In summary, knowledge of the type and date of the preceding therapy is important to correlate any unusual changes not expected in a typical post-SBRT setting. However, if SBRT is performed after intra-arterial therapy or thermal ablation, the findings at follow-up imaging should follow expected post-SBRT findings.

Complications

Complications of SBRT revolve around damage to adjacent organs and adjacent hepatic parenchyma. Severe early toxic effect greater than grade 3 is rare and is seen in 0%–5% of cases. Late toxic effects are slightly more common, with a range of grade 3 toxic effects from 0% to 11% (15,22,64).

Surrounding structures at risk during SBRT include the gastrointestinal tract, skin, and lung (Fig E5). Avoidance of these structures in pretreatment planning is optimal. RILD is less common with SBRT than with whole-liver irradiation. The typical onset is 4–12 weeks after radiation therapy,

Table 2: Features of RILD

Type of Features	Classic RILD	Nonclassic RILD
Setting	Now rare More common in setting of whole-liver irradiation of otherwise healthy livers	Patients with preexisting chronic liver disease Rarely seen in cases after SBRT
Diagnosis	Symptoms of fatigue and abdominal pain Hepatomegaly and ascites at examination Laboratory analysis demonstrates doubling of alkaline phosphatase level with normal bilirubin and transaminase levels	Cirrhotic cases demonstrate Child-Pugh score elevation of ≥2 points Noncirrhotic cases demonstrate change in albumin-bilirubin score, with marked increase in transaminase level (×5) Absence of features of classic RILD

but it can occur months to years after radiation therapy (65). The onset depends on the volume of liver irradiated, cumulative treatment, and hepatic functional reserve (Fig E6).

There are two types described: classic and nonclassic (Table 2). Classic RILD is associated with whole-liver irradiation and is diagnosed on the basis of symptoms, results of clinical examination, and laboratory findings. Nonclassic RILD is seen in the setting of preexisting chronic liver disease and is evident by an increase in the Child-Pugh score or albumin-bilirubin score. Prediction of the development of RILD is difficult. Imaging with elastography before SBRT has demonstrated potential in various studies in predicting the degree of hepatic dysfunction (Fig E7) (66,67).

Conclusion

The role of SBRT in treatment of primary and metastatic liver tumors is expanding. Knowledge of expected post-SBRT imaging features is essential for accurate evaluation of treatment response with an understanding of potential interpretation pitfalls.

***Disclosures of conflicts of interest.*—S.K.V.** Research support from National Institutes of Health (EB001981) (unrelated) and U.S. Department of Defense (W81XWH-19-1-0583-01) (unrelated); textbook royalties from Springer International Publishing.

References

1. Cancer Stat Facts: Liver and intrahepatic bile duct cancer. National Cancer Institute, DCCPS, Surveillance Research Program. https://seer.cancer.gov/statfacts/html/livibd.html. Published 2022. Accessed February 19, 2022.
2. Horn SR, Stoltzfus KC, Lehrer EJ, et al. Epidemiology of liver metastases. Cancer Epidemiol 2020;67:101760.
3. Russell AH, Clyde C, Wasserman TH, Turner SS, Rotman M. Accelerated hyperfractionated hepatic irradiation in the management of patients with liver metastases: results of the RTOG dose escalating protocol. Int J Radiat Oncol Biol Phys 1993;27(1):117–123.
4. Potters L, Kavanagh B, Galvin JM, et al. American Society for Therapeutic Radiology and Oncology (ASTRO) and American College of Radiology (ACR) practice guideline for the performance of stereotactic body radiation therapy. Int J Radiat Oncol Biol Phys 2010;76(2):326–332.
5. Kihlström L, Karlsson B, Lindquist C. Gamma knife surgery for cerebral metastases: implications for survival based on 16 years experience. Stereotact Funct Neurosurg 1993;61(suppl 1):45–50.Do
6. Suramo I, Päivänsalo M, Myllylä V. Cranio-caudal movements of the liver, pancreas and kidneys in respiration. Acta Radiol Diagn (Stockh) 1984;25(2):129–131.
7. Chao ST, Dad LK, Dawson LA, et al. ACR-ASTRO practice parameter for the performance of stereotactic body radiation therapy. Am J Clin Oncol 2020;43(8):545–552.
8. Takeda A, Sanuki N, Eriguchi T, et al. Stereotactic ablative body radiotherapy for previously untreated solitary hepatocellular carcinoma. J Gastroenterol Hepatol 2014;29(2):372–379.
9. Sanuki N, Takeda A, Oku Y, et al. Stereotactic body radiotherapy for small hepatocellular carcinoma: a retrospective outcome analysis in 185 patients. Acta Oncol 2014;53(3):399–404.
10. Wilson RR. Radiological use of fast protons. Radiology 1946;47(5):487–491.
11. Durante M, Loeffler JS. Charged particles in radiation oncology. Nat Rev Clin Oncol 2010;7(1):37–43.
12. Suit H. The Gray Lecture 2001: coming technical advances in radiation oncology. Int J Radiat Oncol Biol Phys 2002;53(4):798–809.
13. Steinberg ML, Konski A. Proton beam therapy and the convoluted pathway to incorporating emerging technology into routine medical care in the United States. Cancer J 2009;15(4):333–338.
14. Apisarnthanarax S, Barry A, Cao M, et al. External beam radiation therapy for primary liver cancers: an ASTRO Clinical Practice Guideline. Pract Radiat Oncol 2022;12(1):28–51.
15. Moore A, Cohen-Naftaly M, Tobar A, et al. Stereotactic body radiation therapy (SBRT) for definitive treatment and as a bridge to liver transplantation in early stage inoperable hepatocellular carcinoma. Radiat Oncol 2017;12(1):163.
16. Katz AW, Chawla S, Qu Z, Kashyap R, Milano MT, Hezel AF. Stereotactic hypofractionated radiation therapy as a bridge to transplantation for hepatocellular carcinoma: clinical outcome and pathologic correlation. Int J Radiat Oncol Biol Phys 2012;83(3):895–900.
17. Walter F, Fuchs F, Gerum S, et al. HDR brachytherapy and SBRT as bridging therapy to liver transplantation in HCC patients: a single-center experience. Front Oncol 2021;11:717792.
18. Mathew AS, Atenafu EG, Owen D, et al. Long term outcomes of stereotactic body radiation therapy for hepatocellular carcinoma without macrovascular invasion. Eur J Cancer 2020;134:41–51.
19. Bujold A, Massey CA, Kim JJ, et al. Sequential phase I and II trials of stereotactic body radiotherapy for locally advanced hepatocellular carcinoma. J Clin Oncol 2013;31(13):1631–1639.
20. Feng M, Suresh K, Schipper MJ, et al. Individualized Adaptive Stereotactic Body Radiotherapy for Liver Tumors in Patients at High Risk for Liver Damage: A Phase 2 Clinical Trial. JAMA Oncol 2018;4(1):40–47.

21. Jang WI, Bae SH, Kim MS, et al. A phase 2 multicenter study of stereotactic body radiotherapy for hepatocellular carcinoma: safety and efficacy. Cancer 2020;126(2):363–372.
22. Méndez Romero A, Wunderink W, Hussain SM, et al. Stereotactic body radiation therapy for primary and metastatic liver tumors: a single institution phase I-II study. Acta Oncol 2006;45(7):831–837.
23. Cárdenes HR, Price TR, Perkins SM, et al. Phase I feasibility trial of stereotactic body radiation therapy for primary hepatocellular carcinoma. Clin Transl Oncol 2010;12(3):218–225.
24. Hong TS, Wo JY, Yeap BY, et al. Multi-institutional phase II study of high-dose hypofractionated proton beam therapy in patients with localized, unresectable hepatocellular carcinoma and intrahepatic cholangiocarcinoma. J Clin Oncol 2016;34(5):460–468.
25. Takeda A, Sanuki N, Tsurugai Y, et al. Phase 2 study of stereotactic body radiotherapy and optional transarterial chemoembolization for solitary hepatocellular carcinoma not amenable to resection and radiofrequency ablation. Cancer 2016;122(13):2041–2049.
26. Kim TH, Koh YH, Kim BH, et al. Proton beam radiotherapy vs. radiofrequency ablation for recurrent hepatocellular carcinoma: a randomized phase III trial. J Hepatol 2021;74(3):603–612.
27. Pollom EL, Lee K, Durkee BY, et al. Cost-effectiveness of stereotactic body radiation therapy versus radiofrequency ablation for hepatocellular carcinoma: a Markov modeling study. Radiology 2017;283(2):460–468.
28. Wahl DR, Stenmark MH, Tao Y, et al. Outcomes After Stereotactic Body Radiotherapy or Radiofrequency Ablation for Hepatocellular Carcinoma. J Clin Oncol 2016;34(5):452–459.
29. Sapir E, Tao Y, Schipper MJ, et al. Stereotactic body radiation therapy as an alternative to transarterial chemoembolization for hepatocellular carcinoma. Int J Radiat Oncol Biol Phys 2018;100(1):122–130.
30. Bush DA, Smith JC, Slater JD, et al. Randomized clinical trial comparing proton beam radiation therapy with transarterial chemoembolization for hepatocellular carcinoma: results of an interim analysis. Int J Radiat Oncol Biol Phys 2016;95(1):477–482.
31. Sanford NN, Pursley J, Noe B, et al. Protons versus photons for unresectable hepatocellular carcinoma: liver decompensation and overall survival. Int J Radiat Oncol Biol Phys 2019;105(1):64–72.
32. Smart AC, Goyal L, Horick N, et al. Hypofractionated radiation therapy for unresectable/locally recurrent intrahepatic cholangiocarcinoma. Ann Surg Oncol 2020;27(4):1122–1129.
33. Nicosia L, Cuccia F, Mazzola R, et al. Stereotactic body radiotherapy (SBRT) can delay polymetastatic conversion in patients affected by liver oligometastases. J Cancer Res Clin Oncol 2020;146(9):2351–2358.
34. Voglhuber T, Eitz KA, Oechsner M, Vogel MME, Combs SE. Analysis of using high-precision radiotherapy in the treatment of liver metastases regarding toxicity and survival. BMC Cancer 2021;21(1):780.
35. Scorsetti M, Comito T, Clerici E, et al. Phase II trial on SBRT for unresectable liver metastases: long-term outcome and prognostic factors of survival after 5 years of follow-up. Radiat Oncol 2018;13(1):234.
36. Song CW, Glatstein E, Marks LB, et al. Biological principles of stereotactic body radiation therapy (SBRT) and stereotactic radiation surgery (SRS): indirect cell death. Int J Radiat Oncol Biol Phys 2021;110(1):21–34.
37. Garcia-Barros M, Paris F, Cordon-Cardo C, et al. Tumor response to radiotherapy regulated by endothelial cell apoptosis. Science 2003;300(5622):1155–1159.
38. Solesvik OV, Rofstad EK, Brustad T. Vascular changes in a human malignant melanoma xenograft following single-dose irradiation. Radiat Res 1984;98(1):115–128.
39. Quarmby S, Kumar P, Kumar S. Radiation-induced normal tissue injury: role of adhesion molecules in leukocyte-endothelial cell interactions. Int J Cancer 1999;82(3):385–395.
40. Timmerman RD, Herman J, Cho LC. Emergence of stereotactic body radiation therapy and its impact on current and future clinical practice. J Clin Oncol 2014;32(26):2847–2854.
41. Abelson JA, Murphy JD, Loo BW Jr, et al. Esophageal tolerance to high-dose stereotactic ablative radiotherapy. Dis Esophagus 2012;25(7):623–629.
42. Nishimura S, Takeda A, Sanuki N, et al. Toxicities of organs at risk in the mediastinal and hilar regions following stereotactic body radiotherapy for centrally located lung tumors. J Thorac Oncol 2014;9(9):1370–1376.
43. Finkelstein SE, Timmerman R, McBride WH, et al. The confluence of stereotactic ablative radiation therapy and tumor immunology. Clin Dev Immunol 2011;2011:439752.
44. Postow MA, Callahan MK, Barker CA, et al. Immunologic correlates of the abscopal effect in a patient with melanoma. N Engl J Med 2012;366(10):925–931.
45. Lugade AA, Moran JP, Gerber SA, Rose RC, Frelinger JG, Lord EM. Local radiation therapy of B16 melanoma tumors increases the generation of tumor antigen-specific effector cells that traffic to the tumor. J Immunol 2005;174(12):7516–7523.
46. Lee Y, Auh SL, Wang Y, et al. Therapeutic effects of ablative radiation on local tumor require CD8+ T cells: changing strategies for cancer treatment. Blood 2009;114(3):589–595.
47. Fajardo LF, Colby TV. Pathogenesis of veno-occlusive liver disease after radiation. Arch Pathol Lab Med 1980;104(11):584–588.
48. Haddad MM, Merrell KW, Hallemeier CL, et al. Stereotactic body radiation therapy of liver tumors: post-treatment appearances and evaluation of treatment response—a pictorial review. Abdom Radiol (NY) 2016;41(10):2061–2077.
49. Olsen C, Welsh J, Kavanagh B, et al. Microscopic and macroscopic tumor and parenchymal effects of liver stereotactic body radiation therapy. Int J Radiat Oncol Biol Phys 2009;73(5):1414–1424.
50. Jonathan EC, Bernhard EJ, McKenna WG. How does radiation kill cells? Curr Opin Chem Biol 1999;3(1):77–83.
51. Price TR, Perkins SM, Sandrasegaran K, et al. Evaluation of response after stereotactic body radiotherapy for hepatocellular carcinoma. Cancer 2012;118(12):3191–3198.
52. Brook OR, Thornton E, Mendiratta-Lala M, et al. CT Imaging Findings after Stereotactic Radiotherapy for Liver Tumors. Gastroenterol Res Pract 2015;2015:126245.
53. Sanuki N, Takeda A, Mizuno T, et al. Tumor response on CT following hypofractionated stereotactic ablative body radiotherapy for small hypervascular hepatocellular carcinoma with cirrhosis. AJR Am J Roentgenol 2013;201(6):W812–W820.
54. Goyal K, Einstein D, Yao M, et al. Cyberknife stereotactic body radiation therapy for nonresectable tumors of the liver: preliminary results. HPB Surg 2010;2010:309780.
55. Mendiratta-Lala M, Masch W, Shankar PR, et al. Magnetic resonance imaging evaluation of hepatocellular carcinoma treated with stereotactic body radiation therapy: long term imaging follow-up. Int J Radiat Oncol Biol Phys 2019;103(1):169–179.
56. Mendiratta-Lala M, Gu E, Owen D, et al. Imaging findings within the first 12 months of hepatocellular carcinoma treated with stereotactic body radiation therapy. Int J Radiat Oncol Biol Phys 2018;102(4):1063–1069.
57. Mendiratta-Lala M, Masch W, Owen D, et al. Natural history of hepatocellular carcinoma after stereotactic body radiation therapy. Abdom Radiol (NY) 2020;45(11):3698–3708.
58. Castilla-Lièvre M-A, Franco D, Gervais P, et al. Diagnostic value of combining 11C-choline and 18F-FDG PET/CT in hepatocellular carcinoma. Eur J Nucl Med Mol Imaging 2016;43(5):852–859.
59. Khan MA, Combs CS, Brunt EM, et al. Positron emission tomography scanning in the evaluation of hepatocellular carcinoma. J Hepatol 2000;32(5):792–797.
60. Solanki AA, Weichselbaum RR, Appelbaum D, et al. The utility of FDG-PET for assessing outcomes in oligometastatic cancer patients treated with stereotactic body radiotherapy: a cohort study. Radiat Oncol 2012;7(1):216.
61. Stinauer MA, Diot Q, Westerly DC, Schefter TE, Kavanagh BD. Fluorodeoxyglucose positron emission tomography response and normal tissue regeneration after stereotactic body radiotherapy to liver metastases. Int J Radiat Oncol Biol Phys 2012;83(5):e613–e618.

62. Huang WY, Kao CH, Huang WS, et al. 18F-FDG PET and combined 18F-FDG-contrast CT parameters as predictors of tumor control for hepatocellular carcinoma after stereotactic ablative radiotherapy. J Nucl Med 2013;54(10):1710–1716.
63. Yu JI, Park HC, Lim DH, et al. The role of diffusion-weighted magnetic resonance imaging in the treatment response evaluation of hepatocellular carcinoma patients treated with radiation therapy. Int J Radiat Oncol Biol Phys 2014;89(4):814–821.
64. Lo CH, Huang WY, Hsiang CW, et al. Prognostic Significance of Apparent Diffusion Coefficient in Hepatocellular Carcinoma Patients Treated with Stereotactic Ablative Radiotherapy. Sci Rep 2019;9(1):14157.
65. Mendiratta-Lala M, Aslam A, Maturen KE, et al. LI-RADS treatment response algorithm: performance and diagnostic accuracy with radiologic-pathologic explant correlation in patients with SBRT-treated hepatocellular carcinoma. Int J Radiat Oncol Biol Phys 2022;112(3):704–714.
66. Lawrence TS, Robertson JM, Anscher MS, Jirtle RL, Ensminger WD, Fajardo LF. Hepatic toxicity resulting from cancer treatment. Int J Radiat Oncol Biol Phys 1995;31(5):1237–1248.
67. Kimura T, Takahashi S, Takahashi I, et al. The time course of dynamic computed tomographic appearance of radiation injury to the cirrhotic liver following stereotactic body radiation therapy for hepatocellular carcinoma. PLoS One 2015;10(6):e0125231.
68. Takamatsu S, Kozaka K, Kobayashi S, et al. Pathology and images of radiation-induced hepatitis: a review article. Jpn J Radiol 2018;36(4):241–256.
69. Lall C, Bhargava P, Sandrasegaran K, et al. Three-dimensional conformal radiation therapy in the liver: MRI findings along a time continuum. J Comput Assist Tomogr 2015;39(3):356–364.
70. Fajardo LF. The unique physiology of endothelial cells and its implications in radiobiology. Front Radiat Ther Oncol 1989;23:96–112.
71. Jung SH, Yu JI, Park HC, Lim DH, Han Y. A feasibility study evaluating the relationship between dose and focal liver reaction in stereotactic ablative radiotherapy for liver cancer based on intensity change of Gd-EOB-DTPA-enhanced magnetic resonance images. Radiat Oncol J 2016;34(1):64–75.
72. Seong J, Kim SH, Suh CO. Enhancement of tumor radioresponse by combined chemotherapy in murine hepatocarcinoma. J Gastroenterol Hepatol 2001;16(8):883–889.
73. Gerena M, Molvar C, Masciocchi M, et al. LI-RADS treatment response assessment of combination locoregional therapy for HCC. Abdom Radiol (NY) 2021;46(8):3634–3647.
74. Lim HS, Jeong YY, Kang HK, Kim JK, Park JG. Imaging features of hepatocellular carcinoma after transcatheter arterial chemoembolization and radiofrequency ablation. AJR Am J Roentgenol 2006;187(4):W341–W349.
75. Sainani NI, Gervais DA, Mueller PR, Arellano RS. Imaging after percutaneous radiofrequency ablation of hepatic tumors. I. Normal findings. AJR Am J Roentgenol 2013;200(1):184–193.